

Optimization and Performance Comparison of Hairpin-Winding PMSM for Electric Vehicles Under Drive Cycle

LIU Huijuan^{1*}, SONG Tengfei¹, DU Jinwen², LIU Bo¹

1. School of Electrical Engineering, Beijing Jiaotong University, Beijing 100044, P. R. China;

2. Electric Engineering Department, Suzhou Inovancel Technology Co., Ltd, Suzhou 215100, P. R. China

(Received 15 July 2021; revised 10 August 2021; accepted 10 September 2021)

Abstract: Aiming at the problem of large AC copper loss caused by skin effects and proximity effects, and low efficiency at high speed of the hairpin-winding permanent magnet synchronous motor (PMSM) for electric vehicles (EVs), this paper firstly established the electromagnetic analytical model of the hairpin winding to calculate AC resistance. And the finite element model (FEM) of the hairpin-winding driving motor is established to calculate the AC characteristic of the hairpin winding at different speeds and temperatures. Then, combining modified particle swarm optimization (MPSO) and FEM, a 60 kW hairpin-winding PMSM is optimized under driving cycle conditions, and the electromagnetic performance and heat dissipation performance are compared with that of the traditional strand-winding motor. Finally, a prototype is made and an experimental platform is built to test the efficiency Map and temperature rise of the hairpin-winding motor over the whole speed range and verify the accuracy of the proposed optimization design method. The results show that the hairpin-winding PMSM not only has higher slot filling rate, high-efficiency range and power density, but also has better heat dissipation performance, which is suitable for application in the field of electric vehicles.

Key words: electric vehicles (EVs); hairpin-winding; optimization design; drive cycle; performance comparison

CLC number: TM315 **Document code:** A **Article ID:** 1005-1120(2021)05-0713-13

0 Introduction

In the new global economy, the electric vehicles (EVs) play an important role in addressing the issue of increasingly environmental pollution. As the key parts of electric vehicles, the electromagnetic and heat dissipation performance of the driving motor directly affect the operating quality and cruising ability of electric vehicles. Therefore, the improvement of the driving motor's power density and efficiency has received considerable critical attention^[1-3].

Recently, hairpin windings, also known as form-wound windings have attracted the attention of motor researchers because of its high slot filling rate and better heat dissipation performance^[4-6]. Ref.[7] compared the efficiency and continuous power-speed trajectory of the traditional strand-winding

and the hairpin-winding induction motors used for EVs in the full speed range, and found that the hairpin-winding induction motor has a higher efficiency range than the strand-winding motor, due to the higher slot filling rate. Ref.[8] used the hairpin-windings motor in the new generation bolt EVs to improve system efficiency, and found that increasing the number of layers of hairpin windings in each slot can effectively reduce its AC eddy current loss. Aiming at the problem of AC eddy loss of hairpin windings, Ref.[9] proposed an asymmetric structure to reduce the AC loss of the hairpin winding at high speed and make the winding current evenly distributed, thereby reducing the hotspot temperature and increasing continuous output capability. But when the motor is at low speed and the DC resis-

*Corresponding author, E-mail address: hjliu@bjtu.edu.cn.

How to cite this article: LIU Huijuan, SONG Tengfei, DU Jinwen, et al. Optimization and performance comparison of hairpin-winding PMSM for electric vehicles under drive cycle[J]. Transactions of Nanjing University of Aeronautics and Astronautics, 2021, 38(5):713-725.

<http://dx.doi.org/10.16356/j.1005-1120.2021.05.001>

tance of each layer of the winding is different, the performance of the motor will be reduced.

Ref. [10] studied the influence of the arrangement mode of hairpin windings in the slots on the current circulation problem. It found that if the conductors in each parallel branch are placed unevenly on each layer, it will lead to uneven distribution of current in two or more branches, causing circulation to increase AC loss and decrease the motor efficiency. To determine the effects of the number of parallel turns and the size of the hairpin winding on the AC loss of the motor at high speed, Ref. [11] conducted numerical analysis on the winding of a section hairpin-winding stator motor. Ref. [12] studied the heat dissipation performance of an oil-cooled hairpin-winding motor, and found that the use of oil injection cooling instead of water jacket cooling can greatly increase the power density and output torque of the hairpin-winding motor.

However, affected by the skin effect and proximity effect^[13], the AC resistance of the hairpin winding will increase sharply at high speed, thereby affecting the output capacity and the motor efficiency in the high-speed range. Therefore, the low DC copper loss at low speed and the high AC copper loss at high speed will complicate the optimization design process of the hairpin-winding motor. How to optimize the comprehensive loss of the hairpin-winding motor under the driving cycle to improve the endurance mileage of EVs has become particularly important.

In view of the above problems, this paper systematically analyzes the AC loss characteristics of hairpin winding, aiming to propose an optimal design method of hairpin-winding motor under certain drive cycle. Firstly, the AC resistance analytical expressions of the hairpin windings at different speeds are deduced and an FEM model is established to calculate the AC resistance characteristics of the hairpin windings. Then, combining the modified particle swarm optimization (MPSO) algorithm with the FEM model, the optimization design method of the hairpin-winding PMSM under the driving cycle is proposed, and a 60 kW hairpin-winding drive motor is optimized. Meanwhile, the electromagnetic and

the heat dissipation performance of optimized hairpin-winding motor is compared with the traditional strand-winding motor. Finally, a hairpin-winding prototype is manufactured and an experimental platform is built to test the electromagnetic and heat dissipation performance of the hairpin-winding motor, so as to verify the feasibility and accuracy of the optimized design method.

1 Structure and Theoretical Analysis

1.1 Hairpin-winding structure

The structures of traditional strand winding and hairpin winding are shown in Fig.1. Because of the reduction of air gap area and insulation area between conductors in the slots, the hairpin windings can effectively improve the slot filling rate and reduce the DC resistance and DC copper loss of stator windings. However, as the area of each layer of winding conductor increases, the eddy current loss of hairpin windings will increase greatly at high speed due to skin effect and proximity effect.

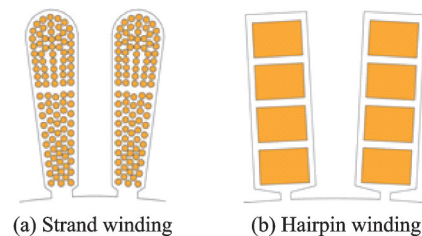


Fig.1 Conventional strand winding and hairpin winding

1.2 Analytical expression of AC resistance

Fig.2 shows the equivalent magnetic structure of hairpin windings. The width and height of stator slots are b_s and h_s , respectively. There are z layers of hairpin conductors in each slot of the stator, and the width and height of each conductor are b_c and h_c , respectively.

The DC resistance R_{DC} of the k th layer hairpin conductor is

$$R_{DC} = \frac{l}{\gamma b_c h_c} \quad (1)$$

where γ is the winding's conductivity. According to Ref. [14], the AC resistance R_{AC} of the k th layer

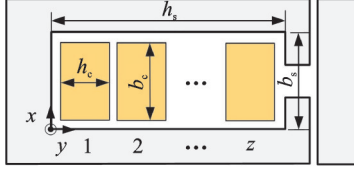


Fig.2 Equivalent structure diagram of hairpin winding

hairpin conductor is

$$R_{AC} = K_{pk} R_{DC} \quad (2)$$

where K_{pk} is the increasing coefficient of AC resistance influenced by skin effect and proximity effect, and its calculation expression is^[14]

$$K_{pk} = \frac{R_{AC}}{R_{DC}} = \varphi(\xi) + k(k-1)\psi(\xi) \quad (3)$$

$$\begin{cases} \varphi(\xi) = \xi \frac{\text{sh}(2\xi) + \sin(2\xi)}{\text{ch}(2\xi) - \cos(2\xi)} \\ \psi(\xi) = 2\xi \frac{\text{sh}\xi - \sin\xi}{\text{ch}\xi + \cos\xi} \\ \xi = \beta h_c \end{cases} \quad (4)$$

where ξ is the relative height of each conductor, $\varphi(\xi)$ the AC resistance coefficient caused by skin effect, and $\psi(\xi)$ the AC resistance coefficient caused by proximity effect. β is the reciprocal of the equivalent penetration depth and its expression is

$$\beta = \sqrt{\pi f \mu \gamma b_c / b_s} \quad (5)$$

where f is the electrical frequency of the winding current and μ the winding permeability.

Since there are a total of z layers hairpin conductors in each slot, it is assumed that all conductors in each slot belong to the same phase, then the average resistance coefficient K_{p1} of hairpin winding is

$$K_{p1} = \frac{1}{z} \sum_{k=1}^z K_{pk} = \varphi(\xi) + \frac{z^2 - 1}{3} \psi(\xi) \quad (6)$$

Similarly, if the conductors in each slot belong to two phases respectively, the average resistance coefficient K_{p21} of the lower winding is^[14]

$$K_{p21} = \varphi(\xi) + \left[\frac{m^2 - 1}{3} \right] \psi(\xi) \quad (7)$$

The average resistance coefficient K_{p22} of the upper winding is^[14]

$$K_{p22} = \varphi(\xi) + \left[\frac{7m^2 - 1}{3} - m^2(1 - \cos\theta) \right] \psi(\xi) \quad (8)$$

where $m = z/2$, $\theta = \pm 60^\circ$.

Based on the above expression, the AC resistance of the hairpin winding can be calculated theoretically at different speeds or electrical frequencies.

2 AC Characteristics of Hairpin Winding

In order to accurately analyze the AC characteristics of the hairpin winding, a 2-D FEM of a 60 kW hairpin-winding PMSM used for EVs is established, as shown in Fig.3. The main performance requirements and parameters of motor are shown in Table 1.

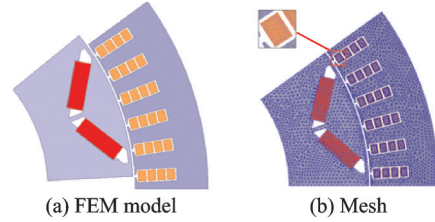


Fig.3 2D-FEM model of hairpin-winding motor

Table 1 Main requirements and parameters of 60 kW PMSM

Parameter	Value	Parameter	Value
DC voltage / V	336	AC voltage / V	220
Max current / A	≤ 400	Max speed/(r•min)	$\geq 10\ 000$
Rated torque/(N•m)	≥ 95	Rated power/ kW	≥ 60
Peak torque/(N•m)	≥ 320	Peak power/ kW	≥ 140
Stator outer parameter/mm	250	Active length/mm	≤ 130
Pole pair	5	Air gap / mm	0.6
Comprehensive loss	Minimum	Torque density	Maximum

2.1 Influence of electrical frequency on AC resistance

Different from the strand winding, the AC resistance of the hairpin winding will change greatly with speed. Fig. 4 presents the intercorrelations (R_{AC}/R_{DC}) between AC/DC resistance ratio and frequency of hairpin windings at 20 °C and 120 °C. Fig. 4 shows that the AC resistance of the hairpin winding increases with the increase of motor speed and frequency due to the skin effect and proximity

effect. The AC resistance of the winding under the highest speed and 120 °C is about 4 times of the DC resistance.

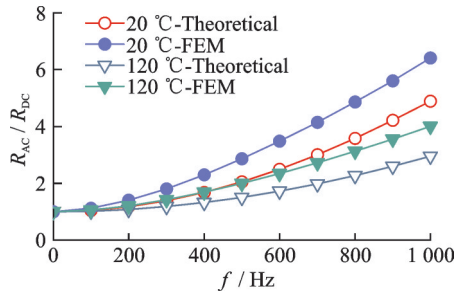


Fig.4 AC/DC resistance ratio vs frequency of hairpin winding

Moreover, because the winding resistivity is greatly affected by temperature, the higher the temperature, the lower resistivity. And according to Eq.(5), it can be seen that the lower the resistivity, the greater the skin depth. Therefore, the growth rate of the AC/DC resistance ratio with the speed at 120 °C is slower than that at 20 °C.

Meanwhile, the theoretical results have a certain deviation from FEM, which is mainly caused by the fact that the theoretical analysis does not consider the core saturation.

Another interesting phenomenon can be found through Eq.(4), that is, each layer of conductor in each slot is affected differently by proximity effect. Fig.5(a) shows the electrical density J distribution diagram of each layer conductor of the hairpin winding at different frequencies by FEM. It can be seen that as the frequency increases, each conductor of the hairpin winding has obvious eddy current effects. And the eddy current effect of the conductor close to the air gap is the most obvious. That is, the eddy loss of the conductor close to the air gap is large, and the current distribution is the most uneven.

Figs.5 (b, c) show the change trend of the AC/DC resistance ratio of each layer of hairpin conductor with frequency and the proportion of AC copper loss of each layer of conductor at different frequencies. Similar to the above conclusions, it can be found that the AC resistance of the conductor close to the air gap has the fastest growth, and the AC copper loss accounts for the highest proportion, ac-

counting for about 58% of the total AC copper loss at the highest speed. The AC resistance of the conductor near the stator yoke increases slowly, and only accounts for about 9% of the total AC copper loss at the highest speed.

This layered characteristic of the hairpin winding makes the AC copper loss distribution of each layer of conductor extremely uneven. It is not conducive to the uniform heat dissipation of the stator windings, which is prone to hot spots, and at the same time increases the risk of excessive temperature rise of air gap.

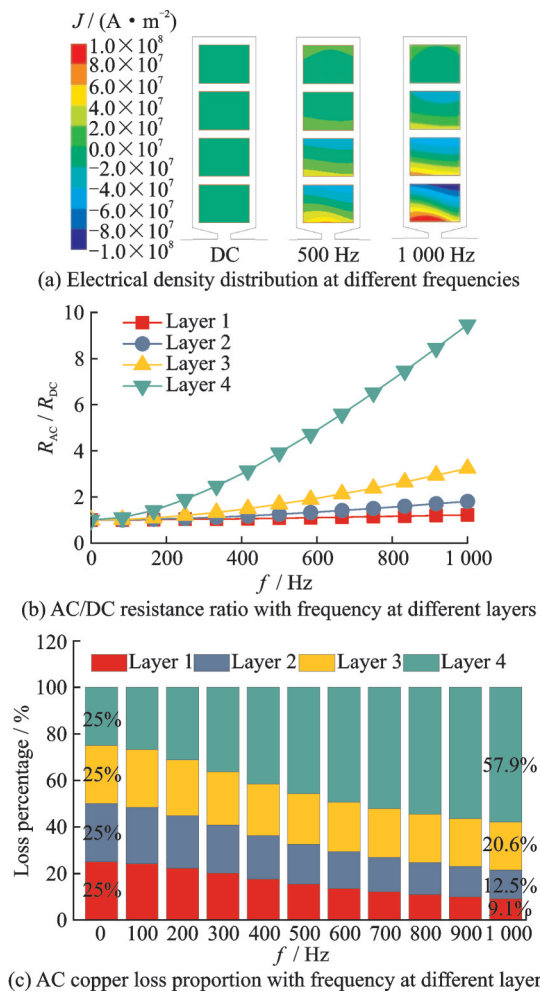


Fig.5 Layered characteristics of hairpin winding

2.2 Influence of winding temperature on AC resistance

Fig.6 shows the change trend of the AC resistance of the hairpin winding with frequency at different winding temperatures. What stands out in Fig.6 is that the DC resistance and the AC resistance at

low frequencies of the hairpin winding increase with the increase of temperature. But as the frequency increases, the tendency of AC resistance to increase with the increasing temperature slows down. The most surprising aspect of the data is in the high frequency (>600 Hz), the AC resistance of the hairpin winding decreases with the increase of winding temperature, which is completely contrary to the change trend of DC resistance.

This result may be explained by the fact that the skin depth of the hairpin windings increases with the increase of temperature and the decrease of electrical conductivity. This phenomenon is beneficial to improving the heat dissipation performance of hairpin-winding motor at high speed and high temperature.

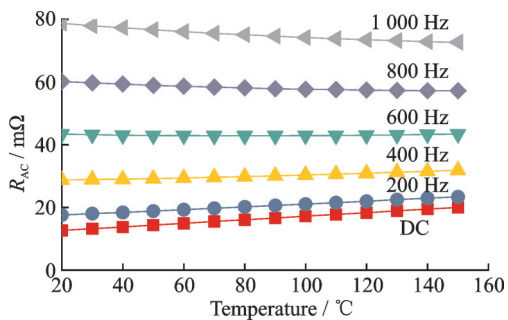


Fig.6 Temperature characteristic of hairpin winding

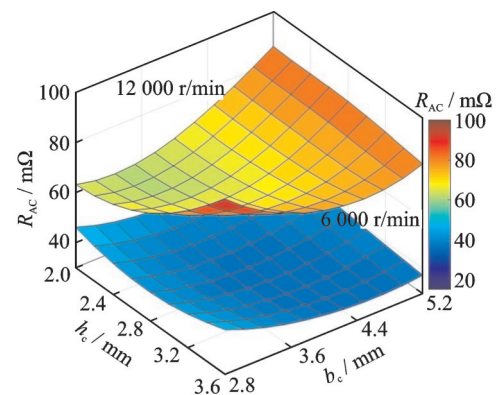
2.3 Influence of winding size on AC resistance

Obviously, the DC resistance and AC resistance of the hairpin winding will be affected by the conductor sizes (height, width). Among them, the larger the cross-sectional area of the winding, the lower the DC resistance. However, AC resistance is not only affected by the winding size, but also by the electric frequency. Fig.7(a) shows the changing trend of AC resistance of the hairpin winding with the conductor width b_c and the width h_c at 6 000 r/min and 12 000 r/min (120 °C). The change trend of AC resistance is different at different speeds. At 6 000 r/min, the AC resistance decreases first and then increases with the increase of the conductor width b_c and the height h_c . But at the high speed of 12 000 r/min, the minimum value of AC resistance appears when the conductor width b_c and the height h_c are the smallest, which is completely opposite to

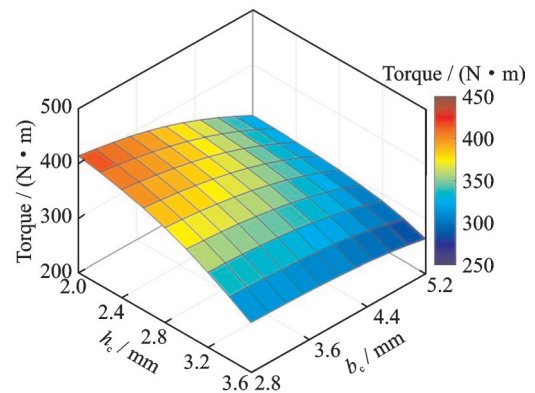
the change trend of the winding DC resistance.

In addition, the change of the winding size will inevitably cause the change of the stator slot size, which will change the torque of the motor. Fig.7(b) shows the change of the output torque of the hairpin-winding motor with the conductor width b_c and the height h_c . The trend shows that the smaller the conductor width b_c and the height h_c , the higher the motor output torque.

Then, how to choose the optimal hairpin winding size has become a complicated problem for multiple working conditions. It is not only necessary to consider the selection of DC resistance in the low-speed range, but also the change in AC resistance in the high-speed range to maximize the overall efficiency of the drive motor.



(a) AC resistance vs winding size at different frequencies



(b) Torque vs winding size at different frequencies

Fig.7 AC loss and torque vs size of hairpin winding

2.4 AC resistance of the end-winding

Since there is no magnetic circuit constraint around the end winding, the AC resistance of the end winding changing with the frequency is different from the effective winding. A 3D FEM of the hair-

pin-winding PMSM is established to calculate the AC resistance of the end winding with different frequencies, as shown in Fig. 8. From the graph we can see that because the end winding is less affected by the proximity effect, its AC resistance increases slowly, which is much lower than the effective winding. As a result, the growth trend of the entire winding's AC resistance decreases.

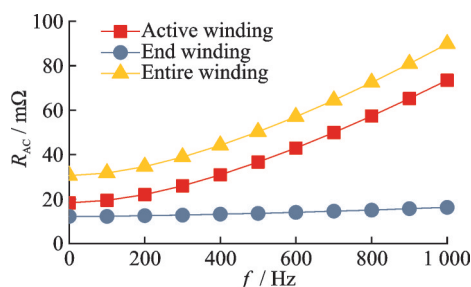


Fig. 8 AC resistance of end winding vs frequency

3 Optimization Design of Hairpin-Winding PMSM

3.1 Number of winding layers

Before optimizing the hairpin-winding PMSM, the number of conductor layers per slot of the hairpin winding must be selected. Fig. 9 presents the structure, slot filling rate and AC resistance of hairpin winding when the motor takes different conductor layers N_s . It can be seen from Fig. 9 that as the number of conductor layers increases, the conductor insulation area in the slot increases, resulting in a decrease in the slot filling rate and a corresponding increase in the DC resistance. But at the same time, the structure of each conductor tends to be flatter, so its AC resistance decreases with the increase of the number of conductor layers at high speed. In order to reduce the DC resistance of the motor and reduce the manufacturing cost, the number of conductor layers of the hairpin-winding motor is selected as four layers in this paper.

3.2 Optimization process

Table 1 shows the constraints and design objectives of the PMSM designed in this paper. It has been previously observed that the main objectives of this optimization are to minimize the comprehensive

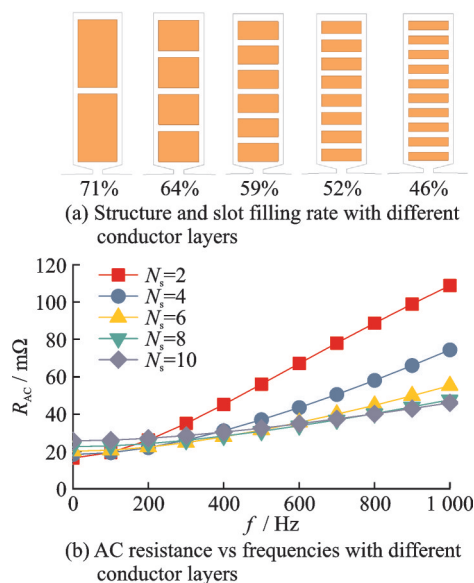


Fig. 9 Characteristics of hairpin with different conductor layers

loss of the motor under certain driving cycle, and to maximize the power density or torque density.

The working condition scatter distribution of the driving motor designed in this paper under the Urban Dynamometer Driving Schedule (UDDS) driving cycle is shown in Fig. 10. From the scatter, it is apparent that the motor mainly works in low-speed (climbing, starting) overload peak operating conditions, long-term medium-speed stable rated operating conditions (5 000 r/min @ 60 kW) and short-term high-speed operating conditions. Therefore, it is necessary to comprehensively consider the losses in these operating conditions in the motor design process to improve cruising range of EVs.

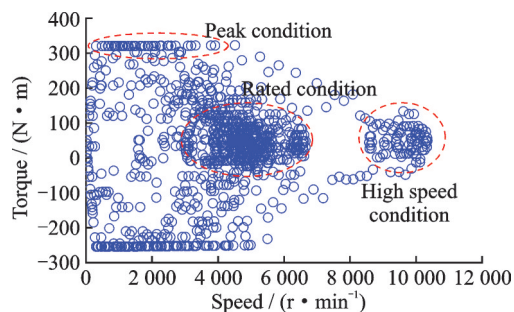


Fig. 10 Working scatter of motor by UDDS cycle condition

However, in the actual optimization design process, it is unrealistic to calculate the loss of all cycle operating points to obtain the comprehensive loss of

the motor. For the purpose of rapid optimization, the center points of the three operating conditions are defined as the rated operating point, the peak operating point and the highest speed operating point, and the equivalent comprehensive loss of the motor under UDDS is defined as

$$\text{Equivalent Loss} = w_r P_{\text{rated}} + w_p P_{\text{peak}} + w_h P_{\text{high}} \quad (9)$$

where P_{rated} , P_{peak} and P_{high} are the total losses of the drive motor at rated operating point, peak operating point and maximum speed point, respectively, including iron loss, AC copper loss, mechanical loss and additional loss. w_r , w_p , and w_h are the weight proportions of the motor under the rated condition, peak condition and maximum speed condition with the UDDS driving cycle, respectively. w_r , w_p , and w_h are obtained by accumulating the power of all operating points in the three regions in Fig.10 and by calculating the proportions.

Fig. 11 shows the flow chart of the optimized design method for the hairpin-winding motor proposed in this paper, which mainly includes three steps:

Step 1 Carrying out the preliminary electromagnetic theoretical design of hairpin-winding motor.

First, analyze the design requirements and design objectives, use the theoretical formulas and design experience to calculate the initial size of the motor, and then use sensitivity analysis to define the optimization variables. The optimization objectives in this paper is to increase the output torque of the motor and reduce the comprehensive loss of the motor. The optimization variables are the inner diameter of the motor stator, the width and the height of the hairpin-winding conductor.

Step 2 Optimizing the torque and comprehensive loss of the motor.

At this step, MPSO^[15] is used to initialize and update the particle swarm population parameters. In the iterative process, the FEM is used to calculate the iron loss, AC copper loss and peak output torque under different parameters, the weight coefficient is used to calculate the comprehensive loss of the motor under the three working conditions and

different size parameters, and MPSO is used for iterative optimization until the design scheme converges.

Step 3 Verification of temperature rise and structural strength.

When the electromagnetic performance of the optimized motor meets the requirements and reaches the optimum, the temperature rise and structural strength of the designed motor are verified.

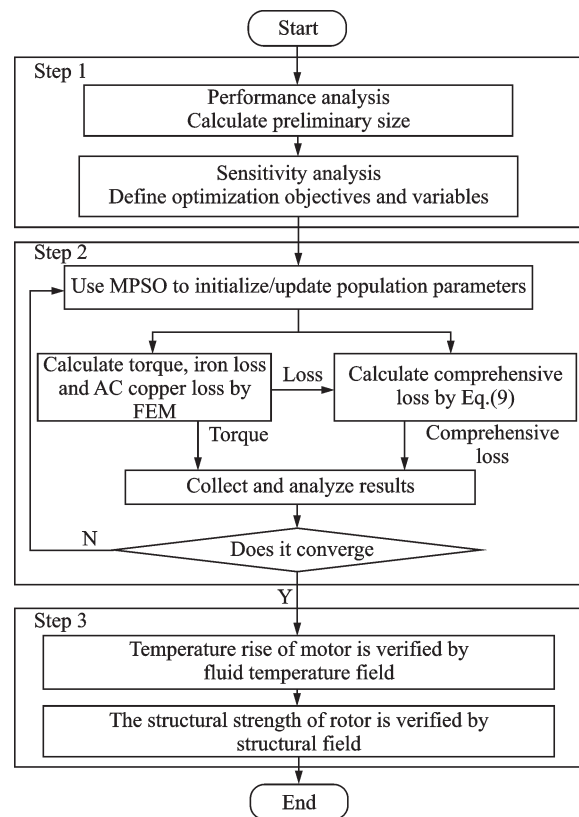


Fig.11 Optimization flow chat

3.3 Optimization results and comparison

Through the method, the performance of the hairpin-windings motor is optimized for multiple iterations. Its comprehensive loss and output torque are optimized, as shown in Fig.12.

It is obvious from Fig.12 that as the optimization progresses, the population gradually approaches to the direction of high torque output and low comprehensive loss, and finally converges to a certain position in space, forming the optimal solution set of the Pareto front.

Table 2 shows the parameter comparison of the hairpin-winding motor before and after optimization.

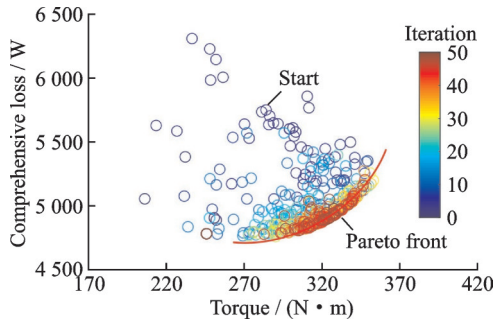


Fig.12 Pareto front and optimal solutions of optimization

Table 2 Parameter comparison of hairpin-winding motor before and after optimization

Parameter	Before	After
Stator ID/mm	177.6	189.7
Conductor width b_c /mm	4.74	4.01
Conductor height h_c /mm	3.61	2.81
Conductor area/mm ²	17.12	11.28
Conductor DC resistance/mΩ	16.8	25.5
Comprehensive loss / W	5 699.7	4 879.6
Peak torque/(N·m)	286.87	321.85

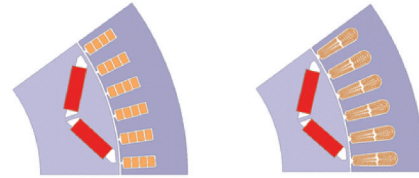
It can be seen that although the winding DC resistance of the hairpin-winding motor increases after optimization, its comprehensive loss decreases from 5 699.7 W to 4 879.6 W and the peak torque is also improved from 286.87 N·m to 321.85 N·m, which verifies the effectiveness of the proposed optimization design method.

4 Comparison of Hairpin-Winding Motor with Strand-Winding Motor

In order to verify the superiority of the performance of the hairpin-winding motor in the field of EVs, this paper also optimizes a strand-winding PMSM under the same restrictive conditions according to the performance requirements of Table 1. The FEM models of the two winding type motors are shown in Fig.13.

Here, the number of conductors per slot of the motor is determined by the current limit, the required output torque and the number of stator slots. Therefore, the number of conductors per slot of the two winding types of motors is the same. The differ-

ence is that the hairpin winding has only one conductor per turn. However, when the number of conductors is determined for the strand-winding motor, the appropriate wire diameter needs to be selected, and each turn of the coil is composed of multiple strand wires.



(a) Hairpin-winding motor (b) Strand-winding motor
Fig.13 Models of hairpin-winding and strand-winding motors

4.1 Electromagnetic performance comparison

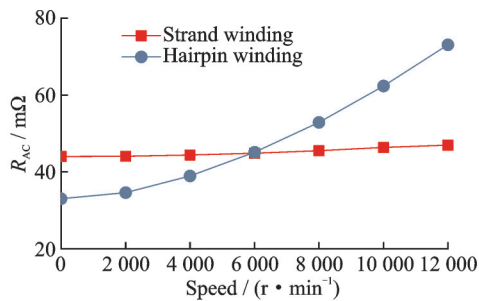
Table 3 shows the comparison of the specific performance parameters of the two winding types of motors, and Fig.14 shows the comparison curves of the AC resistance, and the torque and power external trajectory of the two winding types of motors.

It is apparent from Table 3 that under the same restriction conditions, the hairpin-winding motor has a higher slot full rate and a lower DC resistance value than the strand-winding motor. Therefore, the AC resistance of the hairpin-winding motor in the low speed range ($<6\ 000$ r/min) is smaller. However, when the speed exceeds 6 000 r/min, the AC resistance of the hairpin-winding motor will exceed the strand-winding motor.

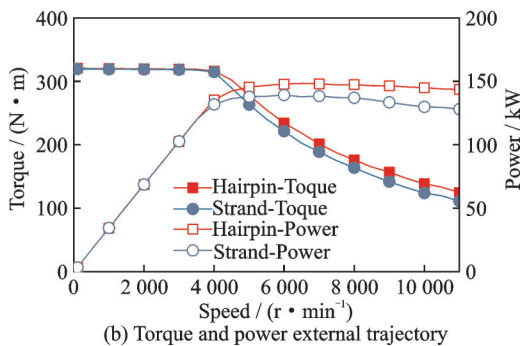
In addition, due to the decrease of the core saturation of the stator teeth, the output torque of the hairpin-winding motor increases and the active length decreases. The reduction of the axial length reduces the no-load back EMF value. Therefore, the flux weakening current of the hairpin-winding motor is small and the peak power is high in the high-speed range. The peak power of the strand-winding motor is 139.2 kW, while the peak power of the hairpin-winding motor is 148.4 kW, which is an increase of 6.6%. In addition, the active length of the hairpin-winding motor is reduced by 10.6%, so the effective power density of the hairpin-winding

Table 3 Comparison of electromagnetic and heat dissipation

Performance parameter	Hairpin-winding motor	Strand-winding motor	Rate of change / %
Slot filling rate / %	64.7	43.2	↑ 21.5
DC resistance / mΩ	25.5	35.3	↓ 27.7
Active length / mm	110	123	↓ 10.6
Peak power / kW	148.4	139.2	↑ 6.6
>85% efficiency area rate / %	92.8	90.1	↑ 2.7
>90% efficiency area rate / %	85.4	80.7	↑ 4.7
Temperature rise at the same loss / °C	64	80	↓ 20
Copper loss at same temperature rise / W	1 384	932	↑ 48



(a) AC resistance under different speeds



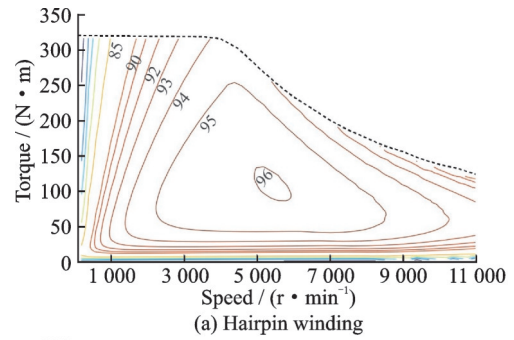
(b) Torque and power external trajectory

Fig.14 Comparison of electromagnetic performance

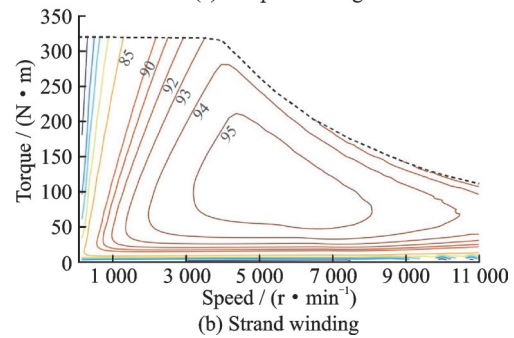
motor is increased by about 19.2% compared with the strand motor.

Fig.15 shows the efficiency map of the two winding types of motors. We can see that efficiency of hairpin-winding motor at low and medium speed range is superior to the traditional strand-winding motor due to the low copper loss and iron loss. However, the efficiency of the hairpin-winding motor is lower than that of the strand-winding motor at high speed range due to the extremely increased AC copper loss. Generally, the high efficiency range of

hairpin-winding motor is significantly higher than that of traditional strand-winding motor, which can make the driving system run more efficiently.



(a) Hairpin winding



(b) Strand winding

Fig.15 Comparison of efficiency map at full speed range

4.2 Thermal performance comparison

In order to verify the heat dissipation performance of the hairpin-winding motor, this paper uses Fluent software to establish the fluid-temperature field simulation model and calculates the steady-state temperature rise of the two winding types of motors.

Table 4 presents all the material properties of motor parts. It is worth noting that due to the complex structure of the strand windings, it is difficult to establish an accurate model of winding in the fluid-temperature field. Therefore, the equivalent method given in Ref.[16] is used to make all strand coils, air gaps and film in each slot of strand winding equivalent to a conductor, and the end of the winding is equivalent to an end ring.

The cooling method of the motor studied in this paper is housing water jacket cooling, and the water channel is the axial Z type. Fig.16 shows the meshing of the fluid-temperature coupling model and the water channel structure. In the simulation, the inlet of the water channel adopts the boundary

Table 4 Material properties of motor parts

Part	Material	Density/ ($\text{kg}\cdot\text{m}^{-3}$)	Thermal conductivity / ($\text{W}\cdot(\text{m}\cdot\text{K})^{-1}$)
Core	35W270	7 800	35/35/1.21
Shell	Aluminum	2 700	168
PMs	N38EH	7 600	420
Shaft	45# steel	7 800	460
Strand winding	Copper(eq)	8 954	0.13/0.13/198
Hairpin winding	Copper	8 954	401
Insulation	Composite	1 400	0.2
Cooling liquid	50% glycol	1 065	0.37

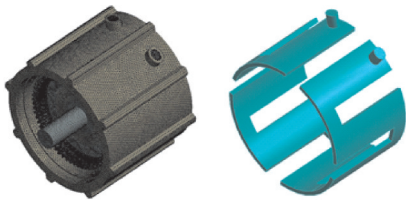


Fig.16 Meshing and cooling channel structure of motor

condition of the flow inlet, the inlet flow is 10 L/min, and the coolant temperature is 60 °C. The outlet adopts the pressure outlet condition, as shown in Table 5.

Table 5 Simulation boundary condition

Parameter	Value
Ambient temperature / °C	60
Inlet boundary condition	Flow inlet
Outlet boundary condition	Pressure outlet
Coolant temperature /°C	60
Coolant inlet flow rate / ($\text{m}\cdot\text{s}^{-1}$)	1.2

Firstly, the two winding types of motors can obtain the same temperature rise (80 °C) by changing the copper loss (other losses are the same), as shown in Fig.17. At this time, the AC copper loss of the hairpin-winding motor is 1 384 W, while the AC copper loss of the strand-winding motor is 932 W. Therefore, the hairpin-winding motor can output higher power under the same steady-state temperature rise limit, which further improves the power density of the motor.

Similarly, the temperature rise distribution of the two motors at the same loss is shown in Fig.18.

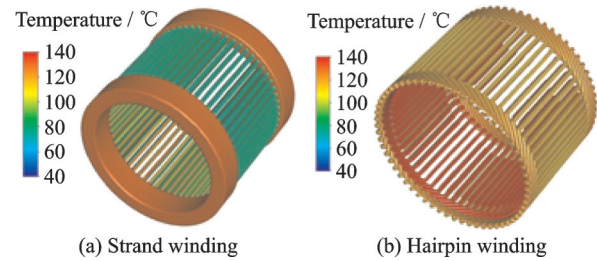


Fig.17 Same steady temperature rises under different losses

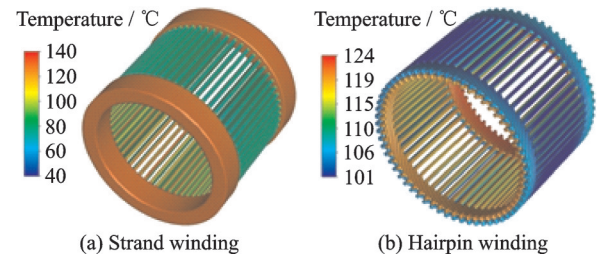


Fig.18 Steady temperature rises under the same losses

It can be known that under the same loss and coolant temperature (60 °C), the steady-state highest temperature rises of the hairpin-winding motor and the strand-winding motor are 124 °C and 140 °C (all appear in the windings), respectively. There is a significant difference between the two winding types of motors, which verifies that the hairpin-winding motor has better heat dissipation performance.

5 Experiment

In order to verify the accuracy of the optimization design method and understand the actual working performance of the hairpin-winding PMSM, a hairpin-winding prototype is manufactured according to the aforementioned design scheme, as shown in Fig.19.

Fig.20 shows the simulated and measured power, torque external trajectory, efficiency and AC copper loss comparison curves. In addition, the AC

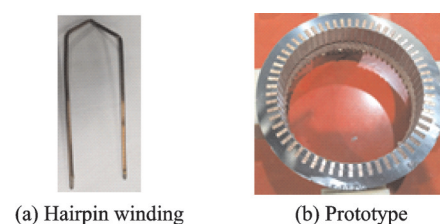


Fig.19 Hairpin winding and prototype

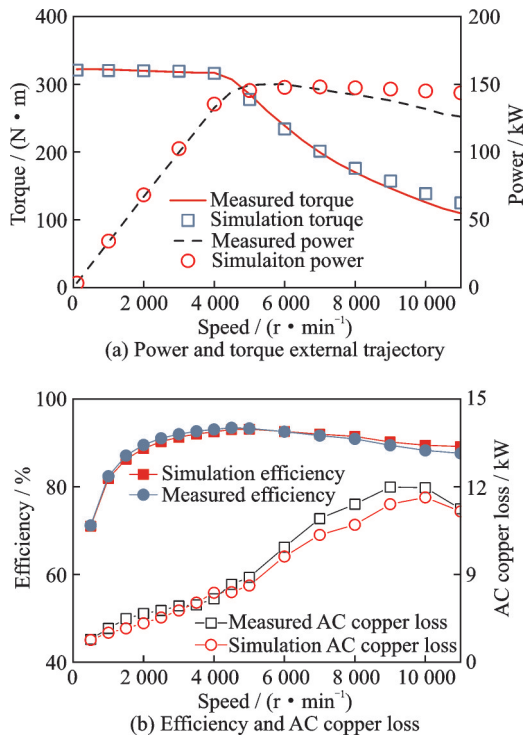


Fig.20 Comparison of simulation and tested characteristic curve

copper loss is calculated by testing the no-load mechanical loss and no-load iron loss, and then through the inverse calculation of the input power and efficiency under load conditions.

We can see from Fig.20 that the simulated torque and power are basically consistent with the measured results at low speed range. However, when the motor is running at high speed, the measured output power is obviously lower than the simulated one, which is mainly caused by the decrease in voltage utilization rate during high-speed testing. The simulated efficiency and AC copper loss are lower than the actual measured results at high speed, which is mainly due to the fact that the high-frequency carrier introduced by the controller is not considered during the simulation.

Fig.21 shows the comparison of simulated and measured steady temperature of the hairpin-winding motor under rated conditions at different positions. The simulation error is basically kept within 10%, which verifies the accuracy of the temperature field simulation in this paper.

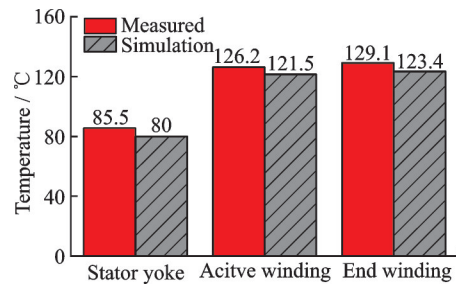


Fig.21 Comparison of temperature of steady condition

6 Conclusions

This paper firstly analyzed the AC characteristics of the hairpin-winding motor through the analytical model and the FEM. Then, combining FEM and the MPSO algorithm, a 60 kW hairpin-winding PMSM is optimized under the UDDS driving cycle. And the optimized results are compared with traditional strand-winding motor in electromagnetic and heat dissipation performance. Finally, the prototype test is used to verified the accuracy of the optimized design method. The main conclusions are as follows:

(1) Affected by the skin effect and proximity effect, the AC resistance of the hairpin winding increases with the increase of the motor speed. And the AC resistance of the effective part of the winding reaches 4—6 times of the DC resistance at the highest speed. Meanwhile, the AC resistance of the hairpin winding will decrease with the increase of temperature at high speed.

(2) The increasing tendency of AC resistance at the hairpin end winding with the increase of speed is slower than that of the effective part, mainly because the end winding is less affected by the proximity effect.

(3) Due to the influence of the eddy effect, the AC resistances of hairpin winding at low speed, medium speed and high speed are completely different with the change of the winding size, resulting in the optimization of hairpin-winding motor becoming a complex multi-condition problem.

(4) Compared with traditional strand-winding motor, the high efficiency range of hairpin-winding motors in the low and medium speed ranges is obvi-

ously better than that of traditional strand motors, but the efficiency at high-speed range is lower due to the larger AC copper loss. In addition, the hairpin-winding motor also has higher peak output power and power density and better heat dissipation performance compared with the strand-winding motor, which is suitable for application in the field of EVs.

References

- [1] EMMA A G, TORBJÖRN T, NIMA S. Acceleration drive cycle efficiency and cost tradeoffs for scaled electric vehicle drive system[J]. *IEEE Transactions on Industry Applications*, 2020, 56(3): 3020-3033.
- [2] YAO X. Performance analysis of vehicle PMSM based on hairpin winding[J]. *Electronic Engineering & Product World*, 2020, 380(9): 43-46.
- [3] YANG Y, CASTANO M, YANG R, et al. Design and comparison of interior permanent magnet motor topologies for traction applications[J]. *IEEE Transactions on Industrial Electronics*, 2017, 3(1): 86-97.
- [4] ISHIGAMI T, TANAKA Y. Motor stator with thick rectangular wire lap winding for HEVs[J]. *IEEE Transactions on Industry Applications*, 2015, 51(4): 2917-2923.
- [5] PARK H J, LIM M S. Design of high power density and high efficiency wound-field synchronous motor for electric vehicle traction[J]. *IEEE Access*, 2019, 1(7): 46677-46685.
- [6] BERARDI G, NATEGH S, BIANCHI N, et al. A comparison between random and hairpin winding in e-mobility applications[C]//*Proceedings of the 46th Annual Conference of the IEEE Industrial Electronics Society*. [S.l.]: IEEE, 2020: 815-820.
- [7] POPESCU M, GOSS J, STATON D A, et al. Electrical vehicles practical solutions for power traction motor systems[J]. *IEEE Transactions on Industry Applications*, 2018, 54(3): 2751-2762.
- [8] MOMEN F, RAHMAN K, SON Y. Electrical propulsion system design of Chevrolet bolt battery electric vehicle[J]. *IEEE Transactions on Industry Applications*, 2018, 55(1): 376-384.
- [9] ISLAM M S, HUSAIN I, AHMED A, et al. Asymmetric bar winding for high-speed traction electric machines[J]. *IEEE Transactions on Transportation Electrification*, 2020, 6(1): 3-15.
- [10] BIANCHI N, BERARDI G. Analytical approach to design hairpin windings in high performance ev motors[C]//*Proceedings of IEEE Energy Conversion Congress and Exposition*. [S.l.]: IEEE, 2018: 4398-4405.
- [11] CHIN J W, CHA K S, PARK M R, et al. High efficiency PMSM with high slot fill factor conductor for heavy-duty EV traction considering AC resistance[J]. *IEEE Transactions on Energy Conversion*, 2020, 36(2): 883-894.
- [12] LIU C, XU Z, GERADA D, et al. Experimental investigation on oil spray cooling with hairpin windings[J]. *IEEE Transactions on Industrial Electronics*, 2020, 67(9): 7343-7353.
- [13] JIANG H. AC loss of flat copper winding in high speed PM motor[J]. *Mechanical & Electrical Engineering*, 2017, 34(9): 1032-1037.
- [14] CHEN S. *Motor design*[M]. Beijing: China Machine Press, 2000: 63-68.
- [15] SONG T F, ZHANG Z Y, LIU H J, et al. Multi-objective optimization design and performance comparison of PMSM for EVs based on FEA[J]. *IET Electric Power Applications*, 2019, 13(8): 1157-1166.
- [16] RAMARATHNAM S, MOHAMMED A K, BILGIN B, et al. A review of structural and thermal analysis of traction motors[J]. *IEEE Transactions on Transportation Electrification*, 2015, 1(3): 255-265.

Acknowledgement This work was supported by the Fundamental Research Funds for the Central Universities (No. 2019YJS181).

Author Prof. LIU Huijuan received the Ph.D. degree in Electrical Engineering from Beijing Jiaotong University in 2009. She worked as a visiting scholar in the Laboratory for Power Electronics & Electrical Machines, the Ohio State University, Columbus, OH, USA, in 2008. In 2011 and 2013, She worked as a research fellow in the Hong Kong Polytechnic University. Since December 2015, she has been a professor in Beijing Jiaotong University. Her current research interests focus on numerical methods of electromagnetic field computation, optimal design and control of high performance electrical machines and novel electrical motors, such as induction machine, doubly fed brushless machine, and permanent magnetic machine for wind power and other new power source development.

Author contributions Prof. LIU Huijuan contributed to

the study, theoretical analysis of the model and prepared the manuscript. Mr. SONG Tengfei and Mr. DU Jinwen contributed to finite element modeling and analysis. Mr. LIU Bo contributed to the discussion and background of the

study. All authors commented on the manuscript draft and approved the submission.

Competing interests The authors declare no competing interests.

(Production Editor: SUN Jing)

循环工况下车用扁铜线绕组永磁同步电机性能优化与对比

刘慧娟¹, 宋腾飞¹, 杜晋文², 刘 博¹

(1. 北京交通大学电气工程学院, 北京 100044, 中国; 2. 苏州汇川技术有限公司电机事业部, 苏州 215100, 中国)

摘要:针对车用扁铜线绕组永磁同步电机高速时绕组中交流损耗大、效率低的问题,首先运用电磁场理论建立扁铜线绕组交流电阻的解析模型,得到定子扁铜线绕组交流电阻的解析表达式,并建立电机有限元模型仿真计算扁铜线绕组在不同转速和不同温度下的交流损耗特性。然后,结合有限元模型和改进粒子群优化算法对一台60 kW 车用扁铜线绕组永磁同步电机进行循环工况下性能优化设计,并将优化后结果与散线绕组电机进行电磁、散热性能对比分析。最后,制作样机并搭建实验平台,测试了扁铜线绕组电机在全转速下的效率Map和温升等性能。结果表明,扁铜线绕组永磁同步电机不仅具有较高的高效区间和功率密度,还具有较好的散热性能,适合应用于电动汽车驱动领域。

关键词:电动汽车;扁铜线绕组;优化设计;循环工况;性能对比